C. Capecchi, S. Min Jo, N. Singh, G. Gori, M. Panesi
Adjoint-Based Sensitivity Analysis for Chemical Non-Equilibrium Kinetics: Application to O2 + O System
in: AIAA Scitech 2024 Forum, AIAA, 2024, ISBN: 9781624107115, p. 1-25, AIAA 2024-0655
[AIAA Scitech 2024 Forum, Orlando, FL, USA, 8-12 Jan. 2024]
doi:10.2514/6.2024-0655

Adjoint-based sensitivity analysis for chemical non-equilibrium kinetics: application to $O_2 + O$ system

Cosimo Capecchi *
Department of Aerospace Science and Technology, Politecnico di Milano, Via La Masa 34, 20156, Milano, Italy

Sung Min Jo †, Narendra Singh ‡
Center for Hypersonics and Entry Systems Studies (CHESS), University of Illinois at Urbana- Champaign, Urbana, Illinois 61801, United States

Giulio Gori §
Department of Aerospace Science and Technology, Politecnico di Milano, via La Masa, 34, 20156 Milano, Italy

Marco Panesi ¶
Center for Hypersonics and Entry Systems Studies (CHESS), University of Illinois at Urbana- Champaign, Urbana, Illinois 61801, United States

This paper investigates the impact of different reaction mechanisms, from dissociation to exchange and inelastic processes, on the evolution of a O_2+O chemical system at non-equilibrium in a 0D reactor at high temperatures. The problem is representative of shock-heated gas and it is of interest for hypersonic applications e.g., to understand the complex thermochemical processes occurring ahead a spacecraft entering the atmosphere. We perform an adjoint-based sensitivity analysis exploiting two different molecular internal models of increasing fidelity. Namely, the rovibrational State-to-State model and the Vibrational-Specific model. The sensitivity to the reaction rates is assessed for the global dissociation rate. Results offer insights concerning the impact of individual reaction coefficients on the objective function, providing an in-depth understanding of their role in the thermochemical evolution of the system.

I. Nomenclature

StS	=	State-to-State model
VS	=	Vibrational-Specific model
QCT	=	Quasi-Classical Trajectory
QSS	=	Quasi-Steady State
t	=	Time
T_e	=	Time when the sensitivity analysis is performed
k_i^D	=	Dissociation Rate of the i^{th} species
k_i^R	=	Recombination Rate of the i^{th} species
k_{ik}^I	=	Inelastic Rate for the process from the i^{th} to the k^{th} species
k_{ik}^E	=	Exchange Rate of the process from the i^{th} to the k^{th} species

*MSc, Department of Aerospace Science and Technology, cosimo.capecchi@mail.polimi.it

†https://orcid.org/0000-0001-6687-0867, Postdoctoral Research Associate, Department of Aerospace Engineering, University of Illinois at Urbana-Champaign, IL, USA, smjo@illinois.edu

‡https://orcid.org/0000-0002-8083-9548, Postdoctoral Research Associate, Department of Aerospace Engineering, University of Illinois at Urbana-Champaign, IL, USA, narsingh@illinois.edu

§https://orcid.org/0000-0001-7442-2773, Assistant Professor, Department of Aerospace Science and Technology, Politecnico di Milano, Via La Masa 34, 20156, Milano, Italy, giulio.gori@polimi.it

¶https://orcid.org/0000-0002-8650-081X, Professor, Department of Aerospace Engineering, University of Illinois at Urbana-Champaign, IL, USA, mpanesi@illinois.edu

K^D_{Glob} = Global dissociation rate
m_i = Mass of the i^{th} species
Y_i = Mass Fraction of the i^{th} species
N = Number of species included in the system
N_p = Number of parameters in adjoint method
$\mathbf{q}$ = Vector-valued function in time
$\mathbf{p}$ = Vector of N_p parameters
μ_r = Relative error
$\mathcal{S}_\nu$ = Vibrational sensitivity reconstructed from StS

II. Introduction

A vehicle traveling at hypersonic speed is subject to extreme thermochemical conditions. Specifically, a large amount of heat is generated as the vehicle flies through the atmosphere at velocities several times the speed of sound. Moreover, a shock wave forms ahead of the vehicle. Across the shock, gas particles are excited to high-energy quantum states, causing the dissociation of molecules and triggering chemical reactions which vary the chemical composition of the gas surrounding the vehicle.

To accurately model such complex flows, state-of-the-art methods embrace a foundation rooted in fundamental principles, with a minimal use of empirical approximations. This approach, known as *ab initio* methodology [1–5]), integrates the first principles of quantum chemistry into computational models. However, it is essential to acknowledge certain key considerations regarding this approach. The *ab initio* methodology relies on several theoretical approximations and statistical techniques. Despite this, it allows the formulation of State-to-State (StS) models [4], where an in-depth description of the kinetic processes can be obtained, especially under strong non-equilibrium conditions, for which the distribution of the internal populations significantly deviates from the Maxwell-Boltzmann distribution. The most detailed StS model is the rovibrational collisional model, where the population of the internal energy levels is computed via the solution of the master equation, solved for each singular level. Therefore, the reaction rates for each each quantum state level are required. The computation of these rates, for a given chemical system, starts by solving Schrödinger's equations under some approximating hypothesis *e.g.*, the Born-Oppenheimer approximation [6], at some specific spatial points. This procedure provides point information about the inter-atomic potential energy. However, the Quasi-Classical Trajectory (QCT) method is used to study the dynamics of the nucleus via Hamilton's equation of motion within a target-projectile framework [7]. The QCT requires the force field in which the nuclei move which can be obtained as the gradient of the potential energy. Therefore, the point information from Schrödinger's equation must be transformed into a continuous differentiable surface with respect to the atomic spatial coordinates i.e., the Potential Energy Surface (PES). Achieving this requires the use of either fitting methods, like Permutation Invariant Polynomials, or interpolation techniques, such as reproducing kernel Hilbert space, see [6, 8]. Once all the QCTs are performed, it is possible to compute the cross-sections of each transition using a Monte Carlo integration to finally compute the reaction rates. Indeed, this can be obtained by integrating the cross-sections over a Maxwellian distribution of translational energies. According to this brief overview, the *ab initio* approach can possibly introduce various sources of error. Nonetheless, this approach serves as the foundation for numerous fundamental analyses in non-equilibrium conditions and lays the groundwork for constructing reduced-order models (ROM), see [9, 10], which are relevant for mitigating the computational cost associated with simulating hypersonic conditions in Computational Fluid Dynamics (CFD).

The goal of this work is to investigate the impact of the dissociation and redistribution reaction rates on the evolution of a 0D chemical reactor under isothermal and isochoric assumptions, specified to the $O_2 + O$ system. The study of the 0D chemical reactor helps to assess the extent to which the sources of error in the *ab initio* approach can affect the physical representation of non-equilibrium flows, a fundamental step for improving our understanding of the evolution of more complex hypersonic applications. In pursuing the paper's goal, we perform an adjoint-based sensitivity analysis of the reaction rates obtained from QCT calculations. The choice of the adjoint-based approach is forced by the huge number of parameters entailed by the challenge of providing a comprehensive description of all quantum state transitions.

The paper is organized as follows. Sec. III describes the reaction processes, the database employed in the sensitivity analysis, and the governing equations used to analyze the evolution of the chemical system. Sec. IV provides the outline of the objective functions undergoing the sensitivity analysis. Sec. V presents two sensitivity analysis methods namely, the Finite Difference and Adjoint Equation methods, and highlights their advantages and drawbacks. Sec. VI describes

the implementation of our analysis framework into a computer code and presents its verification. Sec. VII presents the sensitivity analyses of the considered objective function, using both the StS model and a simpler ROM model. Finally, Sec. VIII summarizes the findings and discusses potential future research.

III. Reaction Processes and Governing Equations

The present work focuses on the study of the $O_2 + O$ chemical system. In this Section, first the reaction processes and the database employed are presented. Then, the governing equations describing the time evolution of the chemical species of the system are reported.

A. Reactions and Database

The database used to carry out the analysis includes 6115 rovibrational energy levels in the electronic ground-state for $O_2(v, J)$, each characterized by the vibrational quantum number v and the rotational quantum number J. These rovibrational states can be sorted by increasing energy and accessed using a single index $i = i(v, J)$, from the set I_{O_2}, with the quantum numbers (v, J), representing each level, ranging from $(0, 0)$ to $(44, 240)$.

For the rovibrational model, the StS rate coefficients are obtained via QCT calculations, performed using COARSEAIR, an in-house QCT code developed within The Center for Hypersonics and Entry System Studies (CHESS) [8, 11, 12] at the University of Illinois at Urbana-Champaign.

In this work, the following set of reaction mechanisms is considered:

- Rovibrational dissociation and recombination processes:

$$O_2(i) + O_C \underset{k_i^D}{\overset{k_i^R}{\rightleftharpoons}} O_A + O_B + O_C.$$

- Rovibrational inelastic, non-reactive, process:

$$O_2(i) + O_C \underset{k_{ik}^I}{\overset{k_{ki}^I}{\rightleftharpoons}} O_2\,(k) + O_C.$$

- Rovibrational exchange process:

$$O_2(i) + O_C \underset{k_{ik}^E}{\overset{k_{ki}^E}{\rightleftharpoons}} O_2\,(k) + O_L, \quad L = A \text{ or } B.$$

The k_i^D, k_i^R, k_{ik}^I and k_{ik}^E are the rate coefficients for dissociation, recombination, inelastic, and exchange processes, respectively, and the pair of index (i, k) represents the rovibrational states for the O_2 molecule.

The forward rates, which include the dissociation and exothermic ones, are computed via QCT calculations, while the backward rates, such as recombination and endothermic ones, are computed by invoking the *microreversibility hypothesis* i.e., detailed balance, using the following relations:

Recombination rates

$$k_i^R = k_i^D \frac{1}{k_i^{eq}} = k_i^D \frac{Q_i(T) Q_{O_2}^t(T)}{\left[Q_O(T) Q_O^t(T)\right]^2},$$

Inelastic/Exchange Endothermic rates

$$k_{ki}^{E,I} = k_{ik}^{E,I} \frac{1}{k_{ik}^{eq}} = k_{ik}^{E,I} \frac{Q_k(T)}{Q_i(T)},$$

where $Q(T)$ and $Q^t(T)$ represent the internal and translational Partition functions, respectively. See Appendix A for the expression of the partition functions.

B. Master Equations

The 0D chemical reactor is an abstract concept that allows to understand how a chemical system, set to given initial conditions, evolves in time. In a 0D reactor, it is assumed that the entire reactor volume can be described as a single, well-mixed "point" or volume element, and therefore no consideration for spatial variations in concentration,

temperature, or other properties within the reactor is taken into account. The set of equations governing the time evolution of the system, under the isochoric and isothermal assumptions, for the rovibrational StS model are Eqs. (1)-(2). This is a set of N ODEs, which takes the name of master equations, which govern the formation and extinction of each chemical species, as a result of different chemical processes. The master equations read:

$$\frac{dY_O}{dt} = \frac{m_O}{\rho}\left[2\sum_{i\in I_{O_2}}\omega_i^D\right] = F_O(Y_O, Y_i, k_i^D), \tag{1}$$

$$\frac{dY_i}{dt} = -\frac{m_i}{\rho}\left[\omega_i^D + \omega_i^E + \omega_i^I\right] = F_i(Y_O, Y_i, k_i^D, k_{ik}^E, k_{ik}^I), \qquad \text{with } i,k \in I_{O_2}, \tag{2}$$

where Y_O and Y_i are the mass fractions of the atomic oxygen and of the $i-th$ level population, respectively, ρ is the density of the chemical mixture and $m_{[]}$ are the masses associated with each species. The mass production terms for the dissociation process ω_i^D, for the exchange process ω_i^E and for the excitation process ω_i^I, are evaluated based on the zeroth-order reaction rate theory, see [13, 14]. Their expressions are

$$\omega_i^D = n_O\left(k_i^D n_i - k_i^R n_O^2\right), \tag{3}$$

$$\omega_i^E = n_O\sum_k\left(k_{ik}^E n_i - k_{ki}^E n_k\right), \tag{4}$$

$$\omega_i^I = n_O\sum_k\left(k_{ik}^I n_i - k_{ki}^I n_k\right). \tag{5}$$

This study aims to perform a sensitivity analysis of the described 0D reactor, using different levels of detail in the treatment of diatomic oxygen. The three distinct models are:

I **Macro**: a simplified and low-level description of the internal molecular structure, which considers the macroscopic representation of the reaction rates. In this approach, molecules are considered bulk entities, and reaction rates are obtained after averaging over internal vibration and specific energy levels. In this work, this model is only used in the phase of verification of the code.

II **StS**: the rovibrational State-to-State model that provides an in-depth and accurate representation of the internal molecular structure. It incorporates not only vibrational energy levels but also rotational ones. The StS model tracks the energy levels specific to each degree of freedom, allowing for a comprehensive understanding of energy transfer and kinetic dynamics.

III **VS**: a ROM, also known as Grouping Strategies, in the *ab initio* State-to-State field. In the VS model, all the levels characterized by the same vibrational quantum number are grouped together. This model provides an enormous reduction in the computational costs, passing from a total of 6115 to 45 states i.e., equations, for the present database, for solving the master equations. Despite the fact that the VS model is shown to be less accurate than other Grouping Strategies, see [12], this model is used since it holds a close representation of the internal molecular structure, given that each group corresponds to a vibrational quantum number.

Further details of the database may be found in Refs. [8, 11, 12].

IV. Objective Functions

In this section, the quantity of interest targeted in the sensitivity analysis is described. Let's consider the 0D isochoric-isothermal chemical reactor, filled with O and O_2. The system is set to the following initial conditions: the molar fractions of the two species, namely X_O and X_{O_2}, are set to 20% and 80%, respectively. The initial thermodynamic condition of the gas *i.e.*, pressure and internal temperature, are set at 1000 Pa and 300 K, respectively. As per the heat-bath temperature, the value is set to 10,000K. The set of reactions includes the dissociation ones, for all three models, and the exchange and excitation processes, for the VS and StS models. The master equations are integrated from 0.0 s to 10^{-5} s.

Figure 1a reports a comparison of the predicted time evolution of the molar fractions O_2 and O. The simplifications introduced in the Macro and VS models are reflected by the differences between the plotted curves. Specifically, the Macro model (solid-blue line) predicts the fastest dynamics, with dissociation and the reaching of the equilibrium

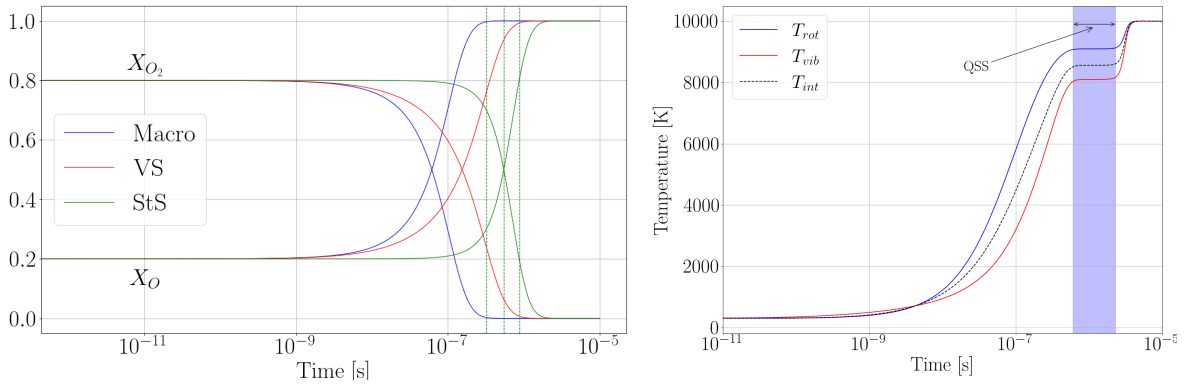

Fig. 1 (a) Molar fractions evolution in time, for each internal molecular structure model. (b) Temporal evolution of rotational, vibrational and internal temperatures of O_2.

condition occurring at the earliest time. This is mainly due to the fact that Macro models O_2 molecules as bulk entities *i.e.*, it completely disregards the internal structure. Shifting focus to the VS model (solid-red line), Fig. 1a reveals that the onset of the O_2 dissociation process aligns with that of the Macro model. In VS, the modeling of 45 internal levels related to vibrational quantum numbers enhances the representation of the non-equilibrium region, especially with the inclusion of redistributive reactions. Despite the advancements over the Macro model, the VS model's accuracy still falls short when compared to the StS model. This limitation primarily stems from the imposition of rotational equilibrium in the formulation of the VS model. As elucidated in Ref. [8], it is revealed that, during the 0D simulations, the population of internal energy levels, computed by the StS simulations, significantly deviates from the equilibrium Maxwell-Boltzmann distribution, meaning that the rotational equilibrium hypothesis results in a misrepresentation of the internal distribution of O_2 during the dissociation process. Therefore, only by assuming both rotational and vibrational non-equilibrium conditions, as in the StS model, it is possible to correctly represent the system evolution.

Another crucial consideration involves the redistribution of energy in the non-equilibrium region when using the StS model. Figure 1b illustrates the behavior of internal (black-dotted line), rotational (blue-solid curve), and vibrational (red-solid line) temperatures as the system progresses toward the equilibrium state. These three temperatures are extracted following the multi-temperature idea, described in Ref. [4]. Specifically, the internal temperature is retrieved from the non-linear equation coupling the internal energy, computed from the weighted summation of each level's energy, to an average energy derived from a Maxwell-Boltzmann distribution. The same idea is used to extract the vibrational and rotational temperatures, with the only difference of that they come from the resolution of a 2x2 non-linear system. Both the non-linear equation and system are solved using the Newton-Raphson method.

Based on Fig. 1b, it is evident and therefore possible to introduce the concept of Quasi-Steady State (QSS) as discussed in [15]. In fact, at high temperatures, the rate of dissociation of O_2 molecules exceeds the relaxation process due to the very effective redistribution of internal populations, especially through the exchange process, creating an overall internal excitation. Specifically, the system lies in a temporary equilibrium condition where the amount of O_2 molecules excited from the highly populated levels is opposed by the depletion of the molecules due to the dissociation process.

The application of StS analysis in the context of CFD simulations is impeded by its large dimensionality. Despite the StS methodology describes the rovibrational energy distribution among molecular species in detail, in CFD simulations the processing of an extensive set of differential equations characterizing each rovibrational state is computationally prohibitive. Therefore the macroscopic representation of the molecules becomes essential. However, great knowledge can be obtained from the evaluation of the StS model. In fact, the computation of macroscopic quantities from the rovibrational energy population is usually performed. In this work, the focus is on the analysis of a macroscopic dissociation rate, which can be obtained as the weighted summation of state-specific dissociation rates

$$K^D_{Glob}(t) = \frac{\sum_i n_i k^D_i}{\sum_k n_k}, \tag{6}$$

where i, k are indices from the set I_{O_2}.

In Appendix C, all the mathematical steps to retrieve the terms required for the adjoint-based sensitivity analysis, reported in the next Section, are provided.

V. Sensitivity analysis methods

The goal of this work is to assess the sensitivity of the global dissociation rate to the different reaction rates, when using different internal molecular models. This is accomplished by computing the gradients of the objective function with respect to the reaction rates. The gradient computation can be performed using two primary methodologies: the finite difference method (FD), first- and second-order accurate, and the adjoint method (ADJ).

A. Finite Difference Method

The finite difference method offers a pragmatic approach for computing sensitivities in systems characterized by complex interdependencies between parameters and variables. In this method, the sensitivity of a target output variable, denoted as G, with respect to a specific parameter p_i, is estimated through discrete perturbations applied to that parameter. Given a function $G(\mathbf{y}, \mathbf{p})$, where $\mathbf{y} \in \mathbb{R}^{\mathrm{N}}$ is the vector of state variables and $\mathbf{p} \in \mathbb{R}^{\mathrm{N_p}}$ the vector of parameter, a perturbation ε is applied to the i-th element of $\mathbf{p}$, resulting in a new vector $\widehat{\mathbf{p}_\mathbf{i}}^{\pm} = \mathbf{p} \pm \varepsilon p_i \mathbf{e_i}$, where e_i is a unit vector in the i-th direction, and the resulting changes in the output variable are used to approximate the sensitivity, using the following discretization formulae:

$$\frac{dG}{dp_i} = \frac{G\left(\mathbf{y}, \widehat{\mathbf{p}_\mathbf{i}}^{+}\right) - G\left(\mathbf{y}, \mathbf{p}\right)}{\varepsilon p_i}, \tag{7}$$

$$\frac{dG}{dp_i} = \frac{G\left(\mathbf{y}, \widehat{\mathbf{p}_\mathbf{i}}^{+}\right) - G\left(\mathbf{y}, \widehat{\mathbf{p}_\mathbf{i}}^{-}\right)}{2\varepsilon p_i}. \tag{8}$$

Eq. (7) represents the first-order approximation formula for the sensitivity, where only a positive perturbation is applied, while Eq. (8) represents the second-order approximation formula, which requires the calculation of the output variable using both the positive and negative perturbations.

Despite its simplicity, the finite difference method is not without limitations. While conceptually straightforward, its computational burden explodes with the number of parameters under consideration. For each parameter, the method requires solving the system of N ODEs multiple times, necessitating an additional N_p resolutions for the first-order finite difference and $2N_p$ resolutions for the second-order finite difference. Consequently, the efficiency of the method diminishes with the number of parameters, shortly becoming impractical for systems described by expensive-to-evaluate models. Moreover, the finite difference method is known to suffer from numerical instability issues. These issues highlight underscore the need for alternative techniques e.g., the adjoint method. Despite its limitations, the finite difference method remains a valuable tool for sensitivity analysis, particularly in cases where a quick and intuitive assessment of the influence of a parameter is required, and whenever the computational cost is not a limiting factor.

B. Single-Time Adjoint Method

The adjoint method allows the efficient computation of the function sensitivity with respect to multiple parameters. This methodology effectively sidesteps the necessity for an exhaustive sequence of simulations, as required by other techniques such as finite difference, by leveraging the concept of duality stemming from minimization problems.

The adjoint method employs a secondary set of ODEs, commonly known as adjoint equations, which act in tandem with the original governing equations, enabling the computation of sensitivities at a significantly reduced computational cost. This distinct feature renders the adjoint method particularly well-suited for systems with a multitude of parameters, where computational efficiency is of paramount importance. Moreover, the adjoint method offers a notable advantage in terms of both accuracy and resource optimization.

In brief, the adjoint method stems from the following minimization problem:

$$\begin{aligned} \mathbf{p}^* = \underset{\mathbf{p}\in\Omega\subset R^{N_P}}{\arg\min} \quad & G\left(\mathbf{y}, \mathbf{p}\right) && = \quad G\left(\mathbf{y}_{T_e}, \mathbf{p}\right), \\ \text{subject to} \quad & \mathbf{h}(\mathbf{y}, \mathbf{y}, \mathbf{p}, t) && = \quad \mathbf{0}, \\ & \mathbf{b}(\mathbf{y}(t_0), \mathbf{p}) && = \quad \mathbf{0}, \end{aligned} \tag{9}$$

where $\mathbf{y}_{T_e}$ represents the master equations solution at the time $t = T_e$. The terms $\mathbf{h}$ and $\mathbf{b}$ represent the implicit form of the governing equations Eqs. (1),(2) and the initial conditions, respectively, that are written as

$$\mathbf{h}(\mathbf{y}, \mathbf{y}, \mathbf{p}, t) = \frac{d\mathbf{y}}{dt} - \mathbf{F}(\mathbf{y}, \mathbf{p}, t) = \mathbf{0}, \tag{10}$$

$$\mathbf{b}(\mathbf{y}(t_0), \mathbf{p}) = \quad \mathbf{y}(t_0) - \mathbf{y}_0 \quad = \mathbf{0}. \tag{11}$$

Following [16], the key is to write the Lagrangian form of the minimization problem, which reads

$$\mathcal{L} = G\left(\mathbf{y}_{T_e}, \mathbf{p}\right) + \int_0^{T_e} \left[\boldsymbol{\lambda}^T \mathbf{h}(\mathbf{y}, \mathbf{y}, \mathbf{p}, t)\right] dt + \boldsymbol{\mu}^T \mathbf{b}(\mathbf{y}_0, \mathbf{p}), \tag{12}$$

where $\boldsymbol{\lambda}$ and $\boldsymbol{\mu}$ represent the vectors of Lagrangian multipliers associated with the set of ODEs and the initial conditions. Since the constraints to the minimization problem (9) are satisfied by construction, the two sets of Lagrangian multipliers are arbitrary. This means that the total derivative of the Lagrangian reads

$$\frac{d\mathcal{L}}{dp} = \frac{dG}{d\mathbf{p}} = \frac{\partial G}{\partial \mathbf{y}_{T_e}} \frac{\partial \mathbf{y}_{T_e}}{\partial \mathbf{p}} + \frac{\partial G}{\partial \mathbf{p}} + \int_0^{T_e} \left(\boldsymbol{\lambda}^T \left[\frac{\partial \mathbf{h}}{\partial \mathbf{y}} \frac{\partial \mathbf{y}}{\partial \mathbf{p}} + \frac{\partial \mathbf{h}}{\partial \dot{\mathbf{y}}} \frac{\partial \dot{\mathbf{y}}}{\partial \mathbf{p}} + \frac{\partial \mathbf{h}}{\partial \mathbf{p}}\right]\right) dt + \boldsymbol{\mu}^T \left[\frac{\partial \mathbf{b}}{\partial \mathbf{y}_0} \frac{\partial \mathbf{y}_0}{\partial \mathbf{p}} + \frac{\partial \mathbf{b}}{\partial \mathbf{p}}\right]. \tag{13}$$

It is possible now to integrate by part the term $\partial\dot{\mathbf{y}}/\partial\mathbf{p}$, which yields to:

$$\begin{aligned} \frac{d\mathcal{L}}{dp} = \frac{\partial G}{\partial \mathbf{p}} + \int_0^{T_e} \left(\left[\boldsymbol{\lambda}^T \left(\frac{\partial \mathbf{h}}{\partial \mathbf{y}} - \frac{d}{dt}\frac{\partial \mathbf{h}}{\partial \dot{\mathbf{y}}}\right) - \dot{\boldsymbol{\lambda}}^T \frac{\partial \mathbf{h}}{\partial \dot{\mathbf{y}}}\right] \frac{\partial \mathbf{y}}{\partial \mathbf{p}} + \boldsymbol{\lambda}^T \frac{\partial \mathbf{h}}{\partial \mathbf{p}}\right) dt + \\ + \left(\frac{\partial G}{\partial \mathbf{y}_{T_e}} + \boldsymbol{\lambda}^T \frac{\partial \mathbf{h}}{\partial \dot{\mathbf{y}}}\right) \frac{\partial \mathbf{y}_{T_e}}{\partial \mathbf{p}} + \left(\boldsymbol{\mu}^T \frac{\partial \mathbf{b}}{\partial \mathbf{y}_0} - \boldsymbol{\lambda}^T \frac{\partial \mathbf{h}}{\partial \dot{\mathbf{y}}}\right) \frac{\partial \mathbf{y}_0}{\partial \mathbf{p}} + \boldsymbol{\mu}^T \frac{\partial \mathbf{b}}{\partial \mathbf{p}}. \end{aligned} \tag{14}$$

In this final form of the Lagrangian (14), the terms multiplying $\partial\mathbf{y}/\partial\mathbf{p}$ have been gathered together either under the integral or for the final and initial time.

Since this expression is to be valid for whatever value of $\partial\mathbf{y}/\partial\mathbf{p}$, by setting the expression between the square brackets under the integral equal to zero, the *Adjoint Equation* is obtained:

$$\dot{\boldsymbol{\lambda}}^T \frac{\partial \mathbf{h}}{\partial \dot{\mathbf{y}}} = \boldsymbol{\lambda}^T \left(\frac{\partial \mathbf{h}}{\partial \mathbf{y}} - \frac{d}{dt}\frac{\partial \mathbf{h}}{\partial \dot{\mathbf{y}}}\right). \tag{15}$$

In the very same fashion, the adjoint expression for the Lagrangian multipliers, which takes into account the effect from the initial conditions $\mathbf{b}$, comes from zeroing out the expression multiplying $\partial\mathbf{y}_0/\partial\mathbf{p}$, *i.e.*:

$$\boldsymbol{\mu}^T \frac{\partial \mathbf{b}}{\partial \mathbf{y}_0} = \dot{\boldsymbol{\lambda}}^T \frac{\partial \mathbf{h}}{\partial \dot{\mathbf{y}}}\,. \tag{16}$$

In the adjoint method, the idea is to integrate backward the adjoint equations (15) from the final time $t = T_e$ to $t = 0$. Therefore an "initial" condition is to be set at $t = T_e$. This condition comes from the round bracket terms multiplying $\partial\mathbf{y}_{T_e}/\partial\mathbf{p}$, which is

$$\boldsymbol{\lambda}^T\left(t = T_e\right) = -\frac{\partial G}{\partial \mathbf{y}_{T_e}} \left(\frac{\partial \mathbf{h}}{\partial \dot{\mathbf{y}}}\right)^{-1}. \tag{17}$$

The remaining terms in Eq. (14) form the expression used for calculating the sensitivity of the problem

$$\frac{dG}{d\mathbf{p}}\left(T_e\right) = \frac{\partial G}{\partial \mathbf{p}} + \int_0^{T_e} \boldsymbol{\lambda}^T \left(\frac{\partial \mathbf{h}}{\partial \mathbf{p}}\right) dt + \boldsymbol{\mu}^T \frac{\partial \mathbf{b}}{\partial \mathbf{p}}. \tag{18}$$

Algorithm 1 expresses the procedure to obtain the sensitivities via the adjoint method. More details can be found in Refs. [17, 18].

Algorithm 1 Adjoint Method Algorithm

Solve the forward problem using the master equations
for all T_e **do**
  Set adjoint equation initial conditions (17)
  for $t = T_e$ **to** $t = 0$ **do**
    Solve adjoint equations, Eq. (15)
    Update adjoint variables at time t
  end for
  Compute the integral within the Eq. (18), using the adjoint variables $\boldsymbol{\lambda}(t)$.
  Sum the contribution $\partial G/\partial \mathbf{p}(t = T_e)$ for each parameter p to compute $dG/d\mathbf{p}(t = T_e)$.
end for

Considering the possible significant differences in scale between G and reaction rates, we simplify the computations for practicality. Therefore, we focus our sensitivity analysis on a modified value that makes the results easier to work with. The calculated sensitivity is:

$$\frac{d\widetilde{G}}{d\widetilde{p}_j}(T_e) = \frac{p_{j,(nom)}}{G(T_e)} \frac{dG}{dp_j}(T_e), \tag{19}$$

where $p_{j,(nom)}$ is the nominal value of the parameter and $G(T_e)$ is the objective function value at $t = T_e$.

C. Advantages and drawbacks

To conclude this brief introduction to the possible choices to perform the sensitivity analysis, in Table 1 we present an overview of the advantages, drawbacks, and computational costs associated with each method. The selection of the ADJ method for this study is rooted in its efficiency and accuracy. Given its ability to compute sensitivities at a reasonable computational effort, even when a large number of parameters is involved, we deem the adjoint method well-suited for the analysis the 0D reactor. However, in this work the FD method is used as a verification tool in Sec. VI.

Method	ODEs	Pros	Cons
Finite Difference 1^{st}	$(N_p + 1)N$	• Does not require access to the simulation's internal equations.	• Computationally expensive. • Prone to numerical inaccuracies.
Finite Difference 2^{nd}	$(2N_p + 1)N$		
Adjoint Method	$(2N + N_p)$	• Very Accurate. • Computational Efficient.	• Not applicable to non-smooth objective functions.

Table 1 Comparison of Methods for Sensitivity Analysis.

VI. Computational tool

In order to perform the presented analysis, we developed and verified a Fortran code to solve the master equations and compute the adjoint-based sensitivities. The code relies on two external libraries:

- PLATO: a thermochemical library (PLAsmas in Thermodynamic nOnequilibrium) [19–21], specifically designed for simulating non-equilibrium plasmas and flows by Dr. A. Munafò from CHESS. The library provided the thermodynamic properties of the chemical system as well as the master equations right-hand-side and Jacobian.
- SUNDIALS: the ODEs integrator, taken from the CVODES solver from SUNDIALS 6.5.0 package [22, 23], is the Backward Differentiation Formulas (BDF), a linear implicit multi-step method, suitable for stiff problems.

Moreover, Equation (15) and Eq. (18) are solved using the ASA module within CVODES, which includes the architecture to perform the backward integration of the adjoint equations.

This section aims at verifying the implementation of the present code. Specifically, two different benchmark tests are presented and their respective results are reported and briefly analyzed.

Section VI.A presents the examination of a simplified scenario for which the analytical solution is available. The analytical results are compared against the ADJ-based sensitivity results, computed using the present code, and the FD approximations. This is performed by quantifying the relative error μ_r between the sensitivity computed analytically and the sensitivity approximated numerically, which is defined as:

$$\mu_r = \frac{\left| \left(\frac{d\widetilde{G}}{d\widetilde{p}} \right)^{\text{Analytic}} - \left(\frac{d\widetilde{G}}{d\widetilde{p}} \right)^{\text{ADJ / FD}} \right|}{\left| \left(\frac{d\widetilde{G}}{d\widetilde{p}} \right)^{\text{Analytic}} \right|} . \tag{20}$$

Next, a second verification text is created by exploiting the first-order Taylor expansion of the objective function G and the sensitivity information computed by the adjoint method, as presented in Sec. VI.B.

A. Macroscopic $O_2 + O$ system without recombination: derivation of the analytical sensitivity

In this simplified case, the molecular oxygen filling the reactor is represented by the Macro model. This implies that the only sensitivity that can be computed is w.r.t. the rate of the single dissociation reaction that governs the system's evolution. Introducing this simplification allows for a cost-effective estimation of sensitivity using the FD method, offering an additional way for cross-validating the results obtained through the ADJ approach. Furthermore, to enable the computation of the analytical solution for the master equation governing this simplified case, the recombination reaction must be artificially excluded, in order to remove the non-linear term multiplying the recombination rate k_i^R.

Since the internal molecular structure is completely neglected, the system is composed only of the macroscopic species, O and O_2, and it is subject only to the following reaction:

$$O_2 + O_C \xrightarrow{k^D} O_A + O_B + O_C \ . \tag{21}$$

Due to these simplifications, the master equations, (1), (2), can be written as:

$$\frac{dY_{O_2}}{dt} = \frac{m_{O_2}}{\rho} \left(-k^D n_O n_{O_2} \right) = -k^D n_O Y_{O_2} = f\left(Y_O, Y_{O_2}\right) \ , \tag{22}$$

$$Y_O = 1 - Y_{O_2} \qquad \text{and} \qquad Y_O = \frac{m_O n_O}{\rho} \ . \tag{23}$$

For the sake of brevity, the analytical expression for the time evolution of the mass fraction of the molecular oxygen is here directly reported. Appendix B provides the complete derivation of this simplified case.

$$Y_{O_2}(t) = \frac{\widetilde{Y}_{O_2} \exp\left(-\frac{\rho}{m_O} k^D t \right)}{1 - \widetilde{Y}_{O_2} + \widetilde{Y}_{O_2} \exp\left(-\frac{\rho}{m_O} k^D t \right)} , \tag{24}$$

where $\widetilde{Y}_{O_2}$ represents the mass fraction of O_2 at t= 0.

Now, it is possible to define a simple objective function G dependent on a single-time instant

$$G\left(t = T_e\right) = Y_{O_2}\left(T_e\right) \ , \tag{25}$$

so that an analytical form can be derived for the sensitivity with respect to the reaction rate

$$\frac{dG}{dk^D}\left(t = T_e\right) = \frac{\rho T_e}{m_O} \left[Y_{O_2}(T_e) - 1 \right] Y_{O_2}(T_e) \ . \tag{26}$$

Here, the results obtained from a 0D isochoric-isothermal chemical reactor filled with atomic and diatomic oxygen are reported. The initial conditions considered for this case are 1000 Pa and 300 K as initial gas pressure and internal temperature respectively. As per the heat-bath temperature, the value is set to 10 000K. The initial molar fractions are set to $X_O = 0.20$ and $X_{O_2} = 0.80$.

In Fig 2, the master equation results obtained by the analytical expression (24) and by the implemented code are represented by the loosely-dashed red and the solid green lines respectively. Moreover, the sensitivity analysis is performed at two different time instants T_e, reported by the two densely-dashed black lines in the same figure.

This first test allows us also to verify the principal advantages and disadvantages documented in Table 1.

Table 2 reports the comparison of the sensitivity results obtained from the analytical expression and ADJ method, showing how the relative error is on the order of 10^{-13}. This proves the very high level of accuracy that characterizes the ADJ method. On the other hand, Fig. 3 highlights that, even though this scenario is very simplified, the maximum order of accuracy reached by the FD method is far from the adjoint one. Furthermore, the accuracy is shown to be strongly related to the perturbation parameter ε, which should be tuned according to the case under analysis and to the discretization formula used.

	Sensitivity [-]	
	$T_e = 9.20 \cdot 10^{-8}$	$T_e = 2.09 \cdot 10^{-7}$
Analytical	$-5.1965813 \cdot 10^{-1}$	$-2.9473543 \cdot 10^{-1}$
Adjoint	$-5.1965813 \cdot 10^{-1}$	$-2.9473543 \cdot 10^{-1}$
μ_r	$9.75 \cdot 10^{-13}$	$1.89 \cdot 10^{-13}$

Table 2 Analytical vs Adjoint Sensitivity Results

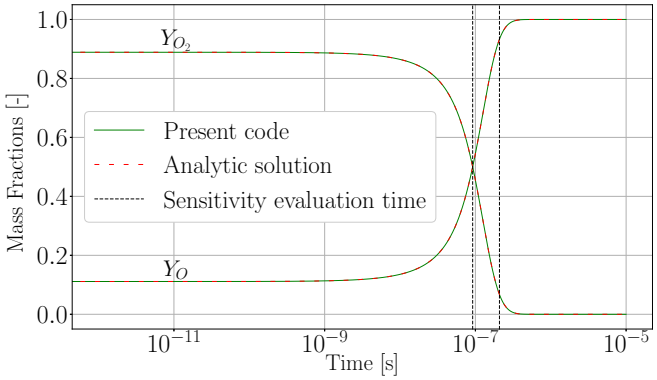

Fig. 2 Mass fractions time evolution: the densely-dashed lines represent the values of time reported in Table 2, the solid line represents the present code solution and the loosely-dashed line represents the analytical solution.

A first observation on the sensitivities emerges. The sensitivity computed with respect to the dissociation rate suggests how the objective function would change if an increase to k^D is applied. Namely, the negative sign of the sensitivity computed for the objective function (25), aligns perfectly with the theoretical expectations. In fact, increasing k^D would increase the pace of O_2 dissociation, leading to a temporal shift of the solution towards the initial time. Therefore, given the time T_e at which the sensitivity analysis is performed, an increase in k^D would imply a lower $Y(T_e)$.

B. Vibrational-Specific model results: relative error and Taylor-expansion-based verification

The second test used to verify the implementation of the code is performed using the VS model and includes both the dissociation/recombination and the redistributive chemical processes. The first part of the test consists of evaluating the sensitivities w.r.t. the 45 reaction rates using both the ADJ and the FD methods and computing the relative error between the two results.

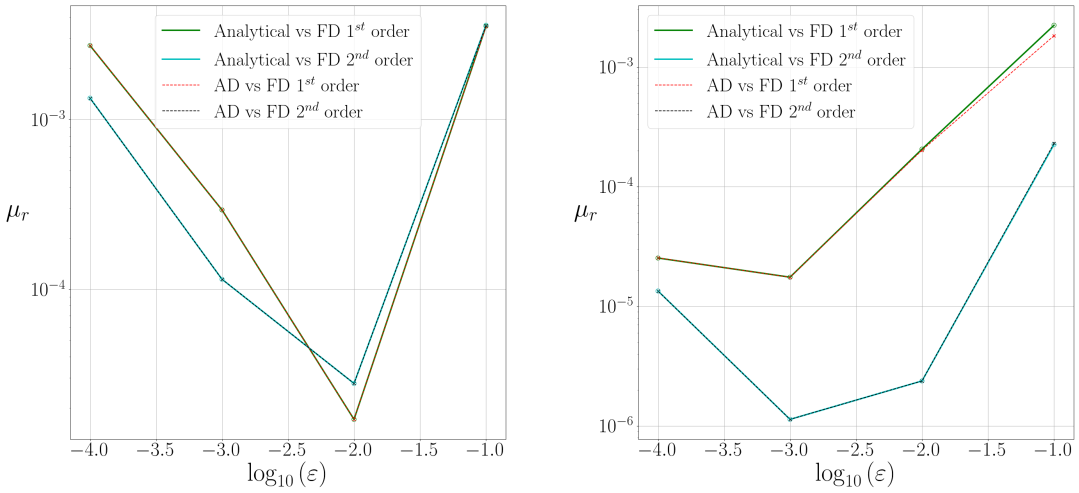

Fig. 3 Relative error between either the analytical and adjoint results with the FD one. (a) $T_e = 9.2 \cdot 10^{-8}$ **s. (b)** $T_e = 2.9 \cdot 10^{-7}$ **s.**

Then, a second investigation of the numerical results can be performed as follows. We first modify one of the reaction rates within the database using a scaling factor denoted as ξ_{scale}, labeled as $k^D_{j,(\text{mod})}$. Then a new 0D simulation is conducted to compute the new objective function value at $t = T_e$, designated as G_{mod}. The relationship between the original and the modified objective functions can be specified using a first-order Taylor expansion as follows:

$$
\begin{aligned}
G_{\text{mod}}\left(\mathbf{y}_{T_e}, k^D_{j,(\text{mod})}\right) &= G_{\text{nom}}\left(\mathbf{y}_{T_e}, k^D_j\right) + \frac{\partial G}{\partial k^D_j}\cdot\delta k^D_j + \frac{\partial G}{\partial \mathbf{y}_{T_e}}\frac{\partial \mathbf{y}_{T_e}}{\partial k^D_j}\cdot\delta k^D_j + \ldots \\
&= G_{\text{nom}}\left(\mathbf{y}_{T_e}, k^D_j\right) + \underbrace{\left[\frac{\partial G}{\partial k^D_j} + \frac{\partial G}{\partial \mathbf{y}_{T_e}}\frac{\partial \mathbf{y}_{T_e}}{\partial k^D_j}\right]}_{\dfrac{dG}{dk^D_j}}\cdot\delta k^D_j + \ldots \\
&= G_{\text{nom}}\left(\mathbf{y}_{T_e}, k^D_j\right) + \left.\frac{dG}{dk^D_j}\right|_{t=T_e}\cdot\delta k^D_j + \ldots
\end{aligned}
\tag{27}
$$

where:

$G_{\text{nom}}\left(\mathbf{y}_{T_e}, k^D_j\right)$: denotes the nominal objective function.

$G_{\text{mod}}\left(\mathbf{y}_{T_e}, k^D_{j,(\text{mod})}\right)$: denotes the modified objective function.

$\dfrac{dG}{dk^D_j}$: indicates the sensitivity of the G with respect to the specific dissociation rate k^D_j.

So, the goal of this second verification test is to retrieve the value of the nominal objective function. Recalling that the sensitivity computed via the adjoint method is adjusted according to the nominal rate and the objective function

value, as in Eq. (19), the expression can be further simplified as follows:

$$
\begin{aligned}
G^*_{\text{nom}} = \quad & G_{\text{mod}} - \left(\frac{dG}{dk_j^D}\right)\Big|_{t=T_e} \cdot \left(k^D_{j,(\text{mod})} - k^D_{j,(\text{nom})}\right) \frac{G_{\text{nom}}(T_e)}{G_{\text{nom}}(T_e)}, \\
= \quad & G_{\text{mod}} - \left(\frac{dG}{dk_j^D}\right)\Big|_{t=T_e} \cdot \frac{k^D_{j,(\text{nom})}}{G_{\text{nom}}(T_e)} \left(\xi_{\text{scale}} - 1\right) G_{\text{nom}}(T_e), \\
= \quad & G_{\text{mod}} - \left(\frac{d\widetilde{G}}{d\widetilde{k}_j^D}\right)\Big|_{t=T_e} \cdot \left(\xi_{\text{scale}} - 1\right) G_{\text{nom}}(T_e),
\end{aligned} \tag{28}
$$

where G^*_{nom} represents the value of the nominal objective function computed using the first-order Taylor expansion and $d\widetilde{G}/d\widetilde{k}_j^D$ is the scaled value of the sensitivity computed via the adjoint method.

The objective function (25) is again considered, with the initial conditions stated in Sec. IV. The FD and ADJ sensitivity results are computed for $T_e = 1.5 \cdot 10^{-7} s$, which is in the middle of the non-equilibrium region, close to the instant at which $X_{O_2} \approx 50\%$ i.e., where the molecular oxygen is undergoing the dissociation and redistribution processes.

The first test is computed using $\varepsilon = 10^{-2}$, over all the 45 rates, while the second one is performed only on four reaction rates, with a scaling factor spanning from $\xi_{scale} = 1/5$ to $\xi_{scale} = 5$. The rates for the second test are chosen so that two have a very high influence on the objective function, namely, the one related to the states $i = 9$ and $i = 24$, while the other two have a very low impact, namely the $i = 0$ and $i = 44$.

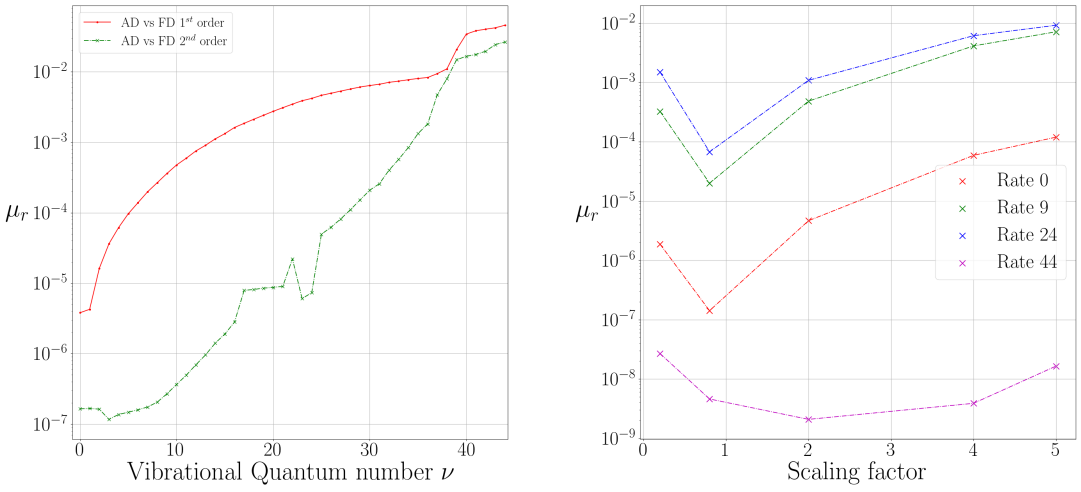

(a) **(b)**

Fig. 4 Verification using the VS model. (a) FD vs. ADJ ($\varepsilon = 10^{-2}$). (b) Relative error between G_{nom} and G^*_{nom}.

Figure 4a presents the relative error between the FD and ADJ methods results. It is clear how the FD method suffers from the very low impact that the high vibrational levels have on the objective function. In fact, the error shows an increasing behavior among the vibrational level, spanning from 10^{-7} for the most influential rates to 10^{-2} for the higher vibrational level rates.

This variation of the relative error according to the reaction rate considered can be noticed also in Fig. 4b. In fact, it can be seen that the truncation of the Taylor expansion to the first order is sufficient for an accurate reconstruction of the nominal objective function when the low influential rates are modified. Specifically, the red and violet curves show a relative error spanning between 10^{-5} and 10^{-9}. On the other hand, the rates that provide a very high impact on the objective function reach an error of the order of 10^{-4}, as depicted by the blue and green curves.

VII. Results

In this section, the results from the previously discussed methodology are presented as follows. In Sec. VII.A, the sensitivities of the global dissociation rate, defined by Eq. (6), with respect to the dissociation rates are reported and analyzed. In Sec. VII.B, the sensitivities of the same objective function with respect to the exchange and inelastic processes are reported. The presented results are the scaled sensitivities, computed using the expression (19).

A. Dissociation Rates Sensitivities

In this subsection, the results from the sensitivity analysis performed on the K^D_{Glob} are presented. Since these sensitivities are related to the the reactions $O_2(i) + O \Longleftrightarrow 3O$, with i representing the i-th internal energy level from the set I_{O_2}, then the presentation of the results follows this idea:

- VS model sensitivities:
  Since the rotational levels are not taken into account, the considered internal levels, and consequently the reaction rates, are just 45, see Sec. III.B. As a result, each sensitivity value is plotted against its corresponding vibrational quantum number, displayed on the x-axis, with the magnitude represented on the y-axis. Notably, results from different time instants are presented in a unified plot, to better show the evolution of the impact of each rate.

- StS model sensitivities:
  To give a better presentation for the 6115 sensitivities computed for the StS model, the idea is to overlay them on the effective diatomic potential of O_2. The potential is presented by plotting the rotational quantum number on the x-axis and the potential energy, expressed in eV, on the y-axis. A color map is used to highlight the different sensitivities impact. The vibrational quantum number can grasped by considering one of the lines in the plot, that starts from $J = 0$, where the lowest indicates the minimum vibrational quantum number $\nu_{min} = 0$ while the highest, the maximum one $\nu_{max} = 44$.

Finally, the VS and StS model results are compared, by reconstructing the vibrational sensitivity from the StS results, following the idea of creating grouped models, see [8]. All the StS levels, associated with the same vibrational quantum number are collected in the set I_ν. So the group-reconstructed sensitivities are obtained from the StS ones via weighted average based on the Boltzmann distribution function f^i_ν over the set I_ν, as follows:

$$\mathcal{S}_\nu(T_e) = \sum_{i \in I_\nu} \frac{d\widetilde{G}}{d\widetilde{k}^D_i}(T_e) f^i_\nu. \tag{29}$$

The Boltzmann distribution is defined as:

$$f^i_\nu = \frac{q_i}{Q_\nu} = \frac{g_i \exp\left(-\dfrac{\varepsilon_i}{K_B T}\right)}{Q_\nu}, \qquad \forall i \in I_\nu,$$

where q_i is the i-th StS level contribution, g_i and ε_i are the degeneracy and the energy of the i-th internal level, respectively, K_B is the Boltzmann constant and T is the translational temperature. Finally, $Q_\nu = \sum_{i \in I_\nu} q_i$ represent the contribution of each group, associated with a vibrational quantum number.

Figure 5 presents the time evolution of the system. On the left y-axis, the molar fraction values, $X_O(t)$ and $X_{O_2}(t)$, are reported using the red-dashed and red-solid lines respectively. On the right y-axis, instead, the magnitude of the global dissociation rate is indicated using the green-solid line. Finally, the black-dotted vertical lines represent the time instants at which the sensitivity analysis is performed.

At first, it is possible to notice how the global dissociation rate computed using the two different models behaves in a very different way. This is mainly due to the hypotheses underlying the construction of the two models. The global dissociation rate at the beginning and at the end of the simulation based on the VS model is the same. Moreover, this value is equal to the equilibrium value retrieved at the end of the StS simulation. This fact is due to the hypotheses at the root of the VS model. Namely, each vibrational level is associated to zero amount of energy. Therefore, both the initial and the equilibrium population represent a Maxwell-Boltzmann distribution and are independent of the temperature. The only differences arise within the non-equilibrium region, where the reaction processes take place.

On the other hand, for the StS model we can see from Fig. 5b that, at the beginning of the simulation, the population distribution is far from equilibrium and shows a very low K^D_{Glob}. As the simulation proceeds, the reaction processes

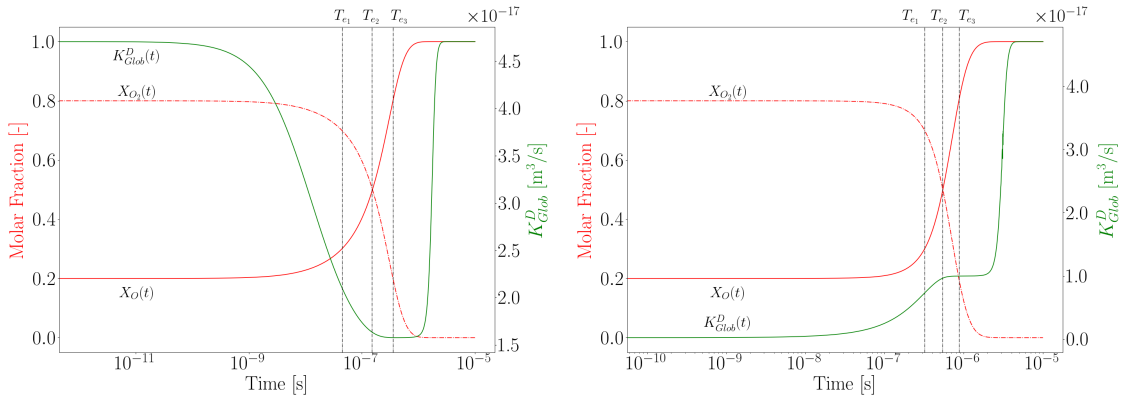

Fig. 5 Evolution in time of the objective function (6)**. Vertical lines: time where the sensitivities are analyzed. (a) VS model. (b) StS model.**

impact the molar fractions of O and O_2 and drive the system to the equilibrium. It is worth noticing that, despite the differences in the time evolution of the two systems, the global dissociation rate, computed with the two models, shows a QSS plateau, as described in Fig. 1b. This is due to the prevalence of chemical reactions over the chemical relaxation of the system.

Three instants in time have been chosen to perform the sensitivity analysis: the first one lies in the region where the dissociation process starts to have an impact on the system's molar fractions so that it can be seen which of the specific reaction rates affects more this early stage of the simulation. Then, a second time instant was selected so that the analysis shows how the rates influence the system when the molar fractions are equal i.e., $X_O = X_{O_2} = 50\%$, and finally the last time instant was chosen so that it lies inside the QSS plateau, which represents the global dissociation rate usually used in the context of the hypersonic CFD simulations. Figure 6 presents a comprehensive examination of sensitivity outcomes for the StS model, providing deeper insights into the system's dynamics.

A notable initial observation is the global positivity of the sensitivities at the chosen time instants. This positive distribution aligns with the behavior of the global dissociation rate, exhibiting a monotonic increasing pattern over time. The positivity implies that alterations in reaction rates systematically impact the increase of the global dissociation rate. Considering the continuous rise of K^D_{glob} over time, changes in reaction rates are expected to correspondingly increase the objective function. This can be grasped intuitively by recognizing that an augmentation in any individual rate hastens the system's convergence toward equilibrium. Consequently, achieving the QSS and the equilibrium occurs earlier, influencing the time when the global dissociation rate reaches its maximum value.

Moreover, it can be demonstrated that, despite the overall stability in sensitivity distribution, the significance of low vibrational levels tends to diminish. This primarily stems from early-stage higher populations, which then move toward equilibrium as the system approaches the QSS plateau due to redistribution processes.

In conclusion, we can affirm that throughout the entire simulation domain the primary influence on the global dissociation rate stems from the dissociation reaction involving reactants within rotational quantum levels ranging from 50 to 180 and possessing a vibrational quantum number laying in the middle-to-low range, as shown by the blue region inside the diatomic potential.

Moving to the VS model, Fig. 7a shows sensitivity results computed at the three instants in time, reported in Fig. 5a. A first major difference can be noticed: if the VS is used to simulate the non-equilibrium within the 0D reactor, the overall positivity of the results, shown for the StS model, is lost. This is primarily due to the different behavior of the K^D_{Glob}. In fact, especially at the first time instant, we can see that the reactions including molecules in the medium-high vibrational levels have a negative impact on the objective function, meaning that they would lead to a steepening of the objective function.

To conclude the analysis related to the sensitivity of the global dissociation rate w.r.t the dissociation rates, Fig. 7b displays the vibrational sensitivities reconstructed from the StS results, using Eq. (29). The most relevant observation, for this comparison, is the different order of magnitude that the sensitivities show: in fact, it is possible to see that the VS model results overestimate the impact of dissociation rates on the objective function. Moreover, it is also possible to

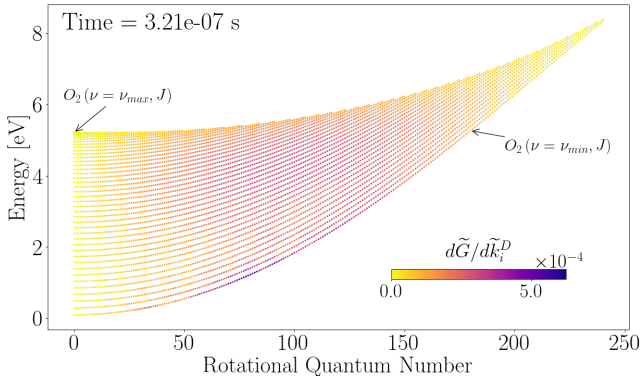

(a)

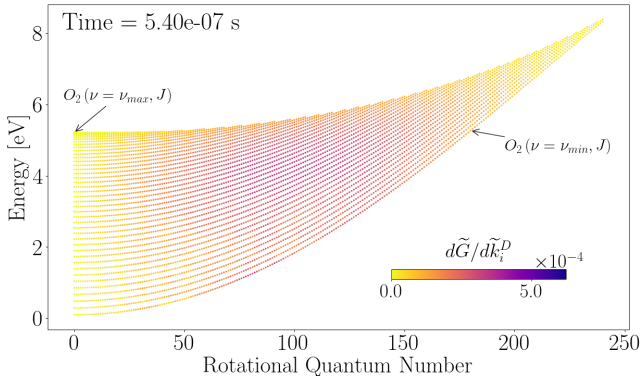

(b)

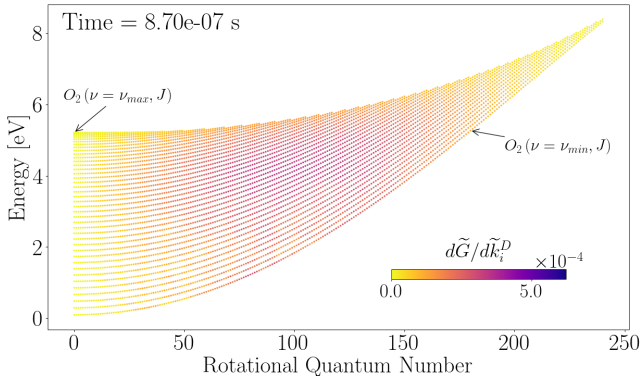

(c)

Fig. 6 Sensitivity results for the StS rovibrational model at the three instants in time shown in Fig. 5b. (a) $T_e = 3.21 \cdot 10^{-7}$**s. (b)** $T_e = 5.430 \cdot 10^{-7}$**s. (c)** $T_e = 8.70 \cdot 10^{-7}$**s.**

see that the effect coming from the higher vibrational levels is not present in the VS model results. This is mainly due to the low populations that these levels have across the entire simulation. Moreover, the reconstruction of the sensitivities benefits the accurate modeling of the non-equilibrium condition provided by the StS model during the simulation.

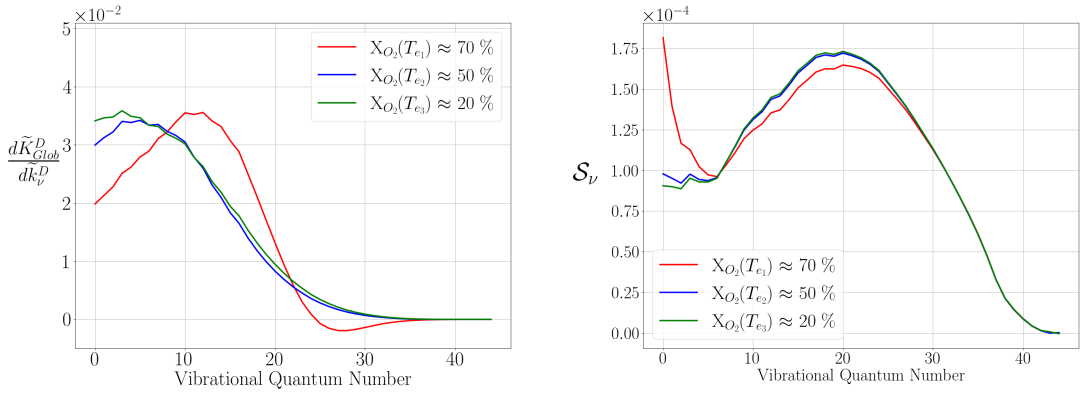

(a) **(b)**

Fig. 7 Comparison of the VS sensitivities with the ones reconstructed from the StS results. (a) VS model. (b) Reconstructed from StS model.

B. Inelastic and Exchange Rates Sensitivities

The sensitivity of the global dissociation rate, Eq. (6), with respect to the exchange and inelastic reaction rates are here reported to complete the analysis.

Figure 8 provides a visual representation of the reaction rates associated with the two distinct processes. A

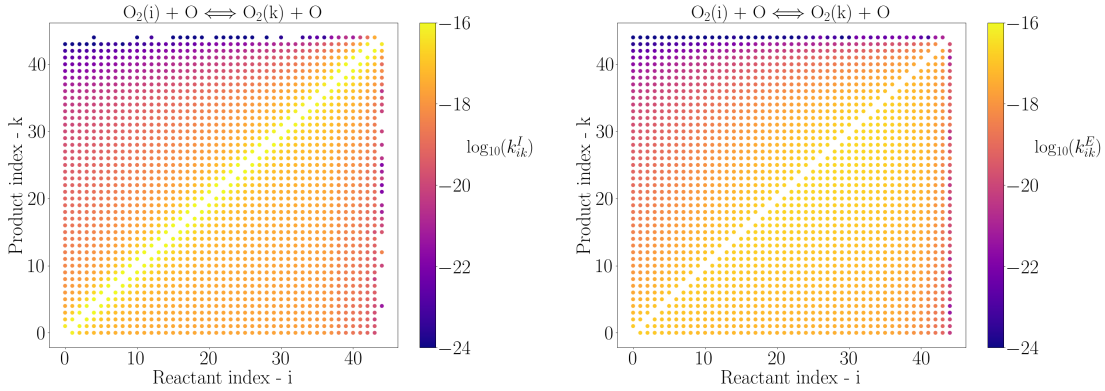

(a) **(b)**

Fig. 8 Rates matrices. (a) Inelastic reaction rates. (b) Exchange reaction rates.

fundamental observation arises upon examination of these rates: they exhibit significant differences in terms of magnitude and distribution. The exchange reactions display a more consistent uniformity across the entire matrix, whereas the inelastic reactions manifest significantly higher rates in regions proximate to the diagonal.

These distinctions in the distribution of rates can be attributed to the underlying physics of the processes involved. Specifically, the inelastic process involves the excitation of rovibrational levels without the breaking of the internal bond between oxygen molecules. On the other hand, the exchange process is characterized by the rupture of the original bond followed by the formation of a new bond with the projectile atom. This fundamental distinction in the nature of the reactions is the root cause of the contrasting rate distributions observed in Fig. 8. The inelastic process, due to its localized excitation mechanism, yields higher reaction rates in the vicinity of the diagonal, whereas the exchange process, involving bond-breaking and formation, exhibits a more consistent distribution across the whole matrix, with a lower maximum magnitude.

The fundamental disparities between the dissociation/recombination processes analyzed in the previous subsection and the inelastic/exchange processes revolve around the redistribution of population among the internal levels of the

reacting species. In the case of dissociation and recombination, these processes involve the breaking and formation of chemical bonds, and they primarily affect the overall concentration of the reacting species. In other words, they significantly impact the total number of molecules involved in the chemical reactions.

On the other hand, inelastic and exchange processes are characterized by different mechanisms. These processes do not result in the creation or annihilation of chemical species but rather in the redistribution of population among the internal energy levels of the molecules. Inelastic processes involve exciting or de-exciting the rovibrational levels of the molecules, which redistributes the energy within the system without altering the total number of molecules. Exchange processes, instead, involve the breaking of an existing O_2 chemical bond, due to the impact with monoatomic oxygen, and the formation of a new O_2 molecule, laying on a different internal level. The distinction in the nature of these processes has implications for the period during which they play a significant role in reactor evolution. The dissociation and recombination processes tend to have a more localized impact in time, as shown by the evolution of the molar fraction, altering the overall concentrations of species. In contrast, inelastic and exchange processes exhibit a more prolonged effect on the system, since they are responsible for distributing the populations to reach the final Maxwell-Boltzmann distribution.

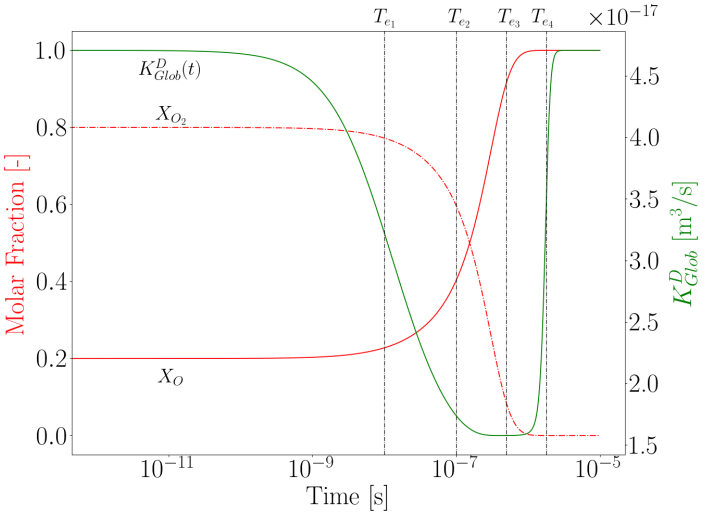

Fig. 9 Objective function Eq. 6 evolution in time for the StS model. Vertical lines: time where the sensitivities are analyzed.

Figure 9, as for the previous analysis, reports the time evolution on the O and O_2 molar fractions, respectively depicted by the red-solid and the red-dash-dotted lines, with the value reported on the left y-axis, while the global dissociation rate over time, presented as the green-solid line and whose behavior is explained in Sec. VII.A, on the right y-axis. Finally, the time four instants at which the sensitivity analysis is performed are reported as the vertical black-dotted lines. These were selected in such a way that the sensitivity analysis could show which redistributive rates are the most influential and how their magnitude changes as the system evolves toward equilibrium.

Figure 10 illustrates the four snapshot results for the sensitivity analysis w.r.t the exchange rates. A notable observation is that the reaction rates responsible for elevating an O_2 molecule from a lower to a higher level i.e., those reactions with $i < k$ (upper-triangular part of the matrices) in the redistribution process, exert a positive influence on the overall dissociation rate. This positive impact is primarily associated with the larger values of the vibrational high-level rates. In fact, by increasing the populations of the level associated with the largest specific dissociation rate K^D_{Glob} increases. Conversely, a decrease in the populations of those levels leads to a reduction in the overall dissociation rate, as supported by the negative sign of the sensitivities in the lower-triangular part of the matrices of Fig. 10.

Furthermore, Fig. 10a shows how the impact of the exchange reaction rates on the objective function, at the early stages of the dissociation process, is mainly due to the exchange of molecules in a vibrational level ranging from 10 to 35. The rates associated with an exchange reaction for which a very large vibrational level variation is achieved, both endothermic and exothermic, are associated with a negligible impact on the global dissociation rate. Figure 8b allows us to state that this very low impact on the objective function is to be associated with the very low magnitude of the rates

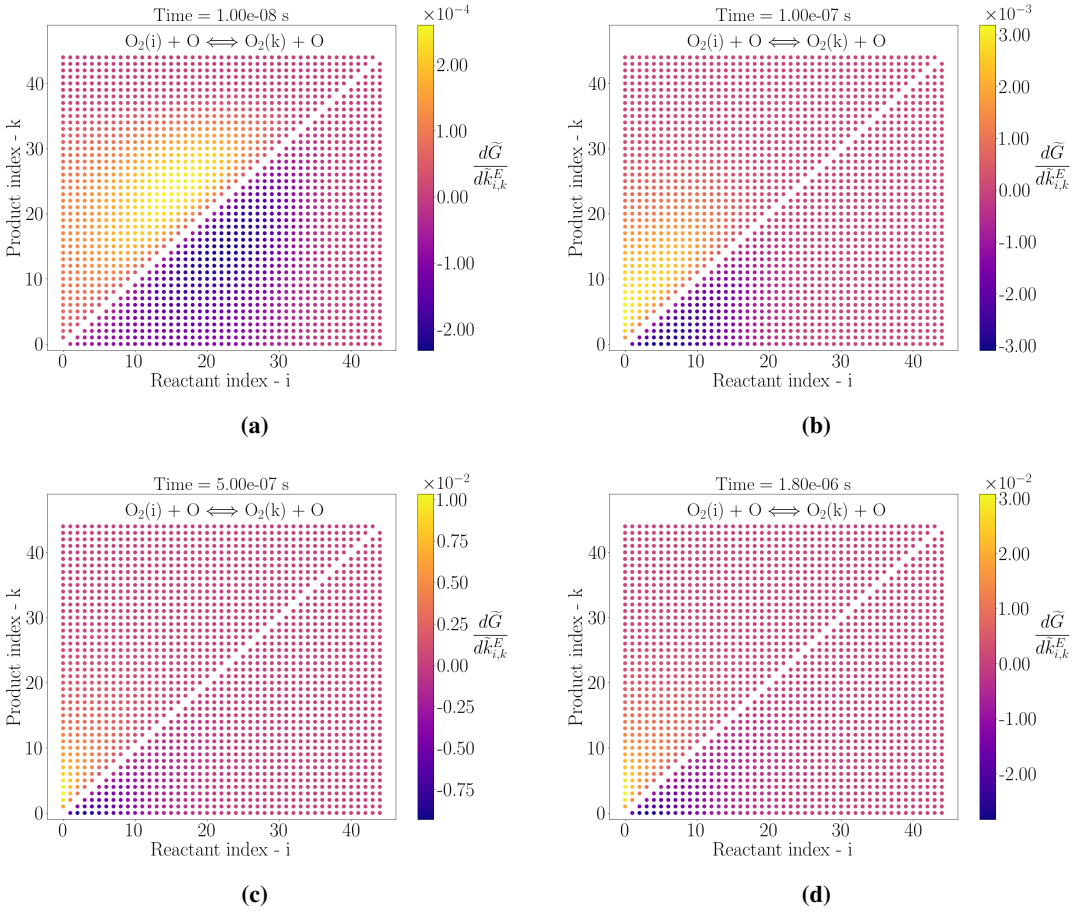

Fig. 10 VS model sensitivity results for the exchange reaction rates k^E_{ik}. (a) $T_e = 1.0 \cdot 10^{-8}$s. (b) $T_e = 1.0 \cdot 10^{-7}$s. (c) $T_e = 5.0 \cdot 10^{-7}$s. (d) $T_e = 1.8 \cdot 10^{-6}$s.

governing these specific reactions.

From Fig. 10b and Fig. 10c, it is possible to note that, as the simulation proceeds, the most relevant parameters affecting the global dissociation rate are the ones involving the redistribution reaction of two O_2 molecules populating the low vibrational levels. Once the QSS plateau is reached, the reaction rates affecting the objective function the most remain the same. In the last snapshot, Fig. 10d, it is possible to see that the magnitude of the sensitivities increases. This agrees with expectations since the redistributive reactions are the processes leading the system in the QSS condition, as explained in [15].

Finally, Fig. 11 shows the four snapshots reporting the sensitivity analysis for the inelastic reaction rates. As per the exchange rates, it is possible to notice the same shift in the sensitivities exerting the most impact of K^D_{Glob}. Moreover, also for this process it is possible to see that the rates associated with an endothermic reaction, *i.e.* $i > k$, have a negative impact (blue color in the figure) on the objective function. This is because such a process removes O_2 molecules from levels associated with higher dissociation rates and redistributes them to levels associated with lower k^D_i. The very opposite reasoning allows us to analyze the sensitivity with respect to rates associated with exothermic reactions *i.e.*, $i < k$.

VIII. Conclusion

This study has established a foundational framework for executing sensitivity analyses in the domain of *ab initio* thermochemistry. The primary objective was to discern the most influential rates in the evolution of a simple chemical system within the context of 0D isothermal and isochoric chemical reactors. To address the challenge, we developed

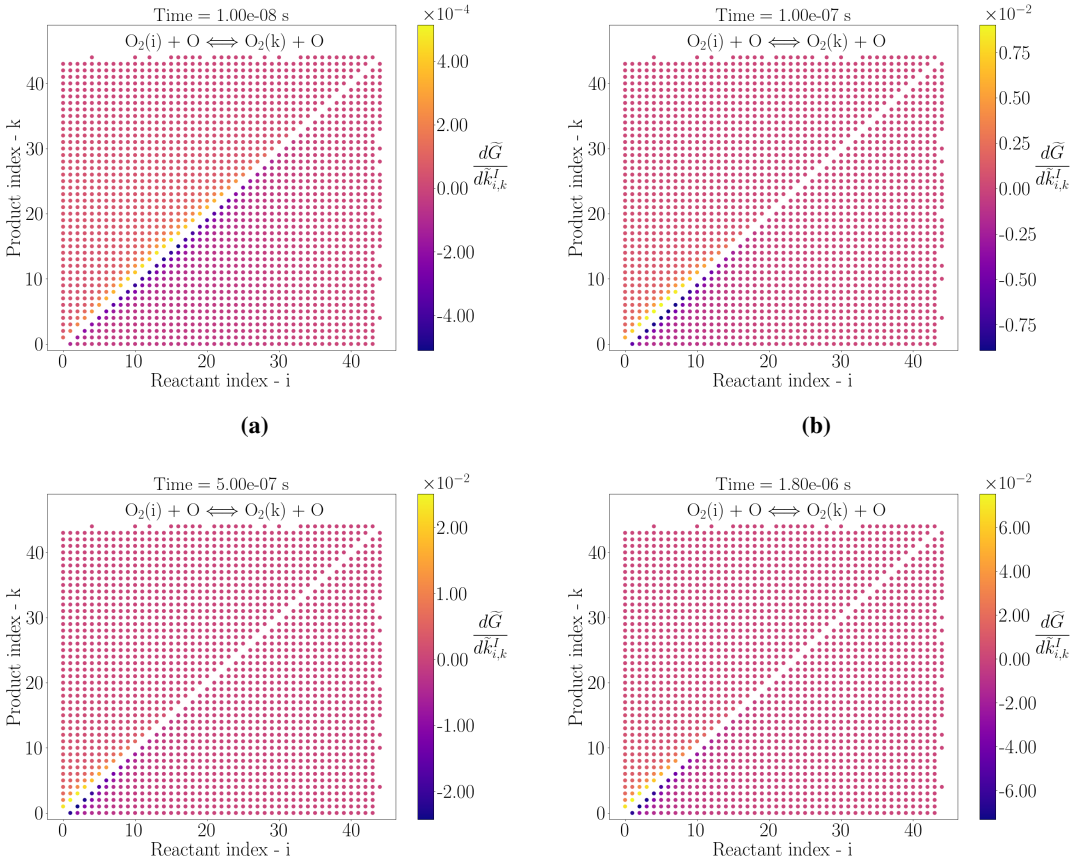

Fig. 11 VS model sensitivity results for the inelastic reaction rates k^I_{ik}. (a) $T_e = 1.0 \cdot 10^{-8}$s. (b) $T_e = 1.0 \cdot 10^{-7}$s. (c) $T_e = 5.0 \cdot 10^{-7}$s. (d) $T_e = 1.8 \cdot 10^{-6}$s.

an adjoint-based computational framework capable of efficiently computing sensitivities for numerous parameters. This framework consists of a FORTRAN code integrating the PLATO thermochemical library and the SUNDIALS suite including ODE solvers and it allows the examination of sensitivities of various reaction parameters and objective functions.

The sensitivity analysis presented in this paper targets the global dissociation rate. The global dissociation rate is widely used in the context of CFD simulation with the aim to characterize the dissociation process of O_2 molecules within the atmospheric model under analysis. The sensitivity analysis is divided into two segments: the examination of the impact of the dissociation rates, as detailed in Sec. VII.A, and the analysis concerning the redistributive rates, reported in Sec. VII.B.

The numerical results obtained from the StS model capture the positive impact of the internal levels dissociation rates. This positivity stems from the definition of the global dissociation rate as (6). A change in one internal level dissociation rate k^D_i has a dual effect on the K^D_{Glob}: a direct impact, due to the presence of the internal levels dissociation rate in the objective function definition, and an indirect one, due to the change in the dissociation process during the non-equilibrium phase of the gas, which affects the internal level populations. Furthermore, a parallel reflection in the sensitivity distribution across internal levels, tied to the population distribution in time, is shown. Specifically, the higher importance of the low-energy levels at the early stages of the simulation is reflected by the higher magnitude of the sensitivity of the objective function to a change of the associated reaction rates. However, as the system evolves in time reaching the QSS region, the magnitude of the sensitivity to low-energy levels reduces in favor of the more highly populated internal states. To complete the sensitivity analysis w.r.t. the dissociation rates, the results obtained using the VS model and the reconstructed vibrational sensitivities from the StS data were compared. The comparison stresses the

limitations of the VS model in representing the impact that each reaction rate has on the global dissociation rate, from both the magnitude and distribution point of view.

Finally, the analysis is completed by computing the sensitivities for the nearly four thousand redistribution rates using the VS model. The numerical results confirm the expectations: the exothermic reaction rates provide a negative impact on K^D_{Glob}. Moreover, the analysis suggests that the set of most influential rates shifts toward the lowest levels as the system evolves to equilibrium.

Future advancements may involve incorporating Automatic Differentiation to enhance flexibility in selecting the objective function. This could also benefit the analysis of adiabatic isochoric reactors, for which the mathematical model includes the energy equations within the master equation. Furthermore, expanding the analysis to chemical systems featuring intricate reaction processes, such as the Zel'dovic reactions in $N_2 + O$ or $O_2 + N$, see [24], represents a promising avenue for future exploration.

Acknowledgments

G. Gori would like to acknowledge that this work was partially supported by the project HERMES funded by the MIUR Progetti di Ricerca di Rilevante Interesse Nazionale (PRIN2022, project n. 2022YPMRNW).

References

[1] Capitelli, M., Armenise, I., Bruno, D., Cacciatore, M., Celiberto, R., Colonna, G., Pascale, O. D., Diomede, P., Esposito, F., Gorse, C., Hassouni, K., Laricchiuta, A., Longo, S., Pagano, D., Pietanza, D., and Rutigliano, M., "Non-equilibrium plasma kinetics: a state-to-state approach," *Plasma Sources Science and Technology*, Vol. 16, No. 1, 2007, p. S30. https://doi.org/10.1088/0963-0252/16/1/S03, URL https://dx.doi.org/10.1088/0963-0252/16/1/S03.

[2] Esposito, F., Armenise, I., and Capitelli, M., "N–N2 state to state vibrational-relaxation and dissociation rates based on quasiclassical calculations," *Chemical Physics*, Vol. 331, No. 1, 2006, pp. 1–8. https://doi.org/https://doi.org/10.1016/j.chemphys.2006.09.035, URL https://www.sciencedirect.com/science/article/pii/S0301010406005441.

[3] Jaffe, R., Schwenke, D., and Panesi, M., *First Principles Calculation of Heavy Particle Rate Coefficients*, 2015, pp. 103–158. https://doi.org/10.2514/5.9781624103292.0103.0158.

[4] Panesi, M., Jaffe, R. L., Schwenke, D. W., and Magin, T. E., "Rovibrational internal energy transfer and dissociation of $N_2(1\Sigma_g^+)N(4S_u)N_2(1\Sigma_g^+)N(4S_u)$ system in hypersonic flows," *The Journal of Chemical Physics*, Vol. 138, No. 4, 2013, p. 044312. https://doi.org/10.1063/1.4774412, URL https://doi.org/10.1063/1.4774412.

[5] Paukku, Y., Yang, K., Varga, Z., and Truhlar, D., "Global ab initio ground-state potential energy surface of N4," *The Journal of chemical physics*, Vol. 139, 2013, p. 044309. https://doi.org/10.1063/1.4811653.

[6] Sharma Priyadarshini, M., "Modeling of boundary layer thermochemistry in hypersonic flows," Ph.D. thesis, University of Illinois at Urbana-Champaign, 2022. URL https://hdl.handle.net/2142/117763.

[7] Karplus, M., Porter, R. N., and Sharma, R. D., "Exchange Reactions with Activation Energy. I. Simple Barrier Potential for (H, H2)," *The Journal of Chemical Physics*, Vol. 43, No. 9, 2004, pp. 3259–3287. https://doi.org/10.1063/1.1697301, URL https://doi.org/10.1063/1.1697301.

[8] Venturi, S., "Machine learning and uncertainty quantification framework for predictive ab initio Hypersonics," Ph.D. thesis, University of Illinois at Urbana-Champaign, 2021. URL http://hdl.handle.net/2142/110403.

[9] Macdonald, R. L., Jaffe, R. L., Schwenke, D. W., and Panesi, M., "Construction of a coarse-grain quasi-classical trajectory method. I. Theory and application to N2–N2 system," *The Journal of Chemical Physics*, Vol. 148, No. 5, 2018, p. 054309. https://doi.org/10.1063/1.5011331, URL https://doi.org/10.1063/1.5011331.

[10] Macdonald, R. L., Grover, M. S., Schwartzentruber, T. E., and Panesi, M., "Construction of a coarse-grain quasi-classical trajectory method. II. Comparison against the direct molecular simulation method," *The Journal of Chemical Physics*, Vol. 148, No. 5, 2018, p. 054310. https://doi.org/10.1063/1.5011332, URL https://doi.org/10.1063/1.5011332.

[11] Venturi, S., Jaffe, R. L., and Panesi, M., "Bayesian Machine Learning Approach to the Quantification of Uncertainties on Ab Initio Potential Energy Surfaces," *The Journal of Physical Chemistry A*, Vol. 124, No. 25, 2020, pp. 5129–5146. https://doi.org/10.1021/acs.jpca.0c02395, URL https://doi.org/10.1021/acs.jpca.0c02395, pMID: 32463672.

[12] Venturi, S., Sharma, M. P., Lopez, B., and Panesi, M., "Data-Inspired and Physics-Driven Model Reduction for Dissociation: Application to the O2 + O System," *The Journal of Physical Chemistry A*, Vol. 124, No. 41, 2020, pp. 8359–8372. https://doi.org/10.1021/acs.jpca.0c04516, URL https://doi.org/10.1021/acs.jpca.0c04516, pMID: 32886505.

[13] Giovangigli, V., "Multi-Component Flow Modeling," *Science China Mathematics*, Vol. 55, 2012. https://doi.org/10.1007/s11425-011-4346-y.

[14] Nagnibeda, E., and Kustova, E., *Non-equilibrium reacting gas flows. Kinetic theory of transport and relaxation processes. Translated from the Russian*, 2009. https://doi.org/10.1007/978-3-642-01390-4.

[15] Andrienko, D. A., and Boyd, I. D., "Rovibrational energy transfer and dissociation in O2–O collisions," *The Journal of Chemical Physics*, Vol. 144, No. 10, 2016, p. 104301. https://doi.org/10.1063/1.4943114, URL https://doi.org/10.1063/1.4943114.

[16] MacArt, J. F., "PDE-Constrained Optimization Using the Adjoint Method," , 2023.

[17] Cao, Y., Li, S., and Petzold, L., "Adjoint sensitivity analysis for differential-algebraic equations: algorithms and software," *Journal of Computational and Applied Mathematics*, Vol. 149, No. 1, 2002, pp. 171–191. https://doi.org/https://doi.org/10.1016/S0377-0427(02)00528-9, URL https://www.sciencedirect.com/science/article/pii/S0377042702005289, scientific and Engineering Computations for the 21st Century - Me thodologies and Applications Proceedings of the 15th Toyota Conference.

[18] Errico, R. M., "What Is an Adjoint Model?" *Bulletin of the American Meteorological Society*, Vol. 78, No. 11, 1997, pp. 2577 – 2592. https://doi.org/https://doi.org/10.1175/1520-0477(1997)078<2577:WIAAM>2.0.CO;2, URL https://journals.ametsoc.org/view/journals/bams/78/11/1520-0477_1997_078_2577_wiaam_2_0_co_2.xml.

[19] Munafò, A., and Panesi, M., "Plato: a high-fidelity tool for multi-component plasmas," 2023. https://doi.org/10.2514/6.2023-3490.

[20] Munafò, A., Alberti, A., Pantano, C., Freund, J., and Panesi, M., "Modeling of Laser-Induced Breakdown Phenomena in Non-Equilibrium Plasmas," 2018. https://doi.org/10.2514/6.2018-0171.

[21] Munafò, A., Alberti, A., Pantano, C., Freund, J., and Panesi, M., "A computational model for nanosecond pulse laser-plasma interactions," *Journal of Computational Physics*, Vol. 406, 2019, p. 109190. https://doi.org/10.1016/j.jcp.2019.109190.

[22] Gardner, D. J., Reynolds, D. R., Woodward, C. S., and Balos, C. J., "Enabling new flexibility in the SUNDIALS suite of nonlinear and differential/algebraic equation solvers," *ACM Transactions on Mathematical Software (TOMS)*, 2022. https://doi.org/10.1145/3539801.

[23] Hindmarsh, A. C., Brown, P. N., Grant, K. E., Lee, S. L., Serban, R., Shumaker, D. E., and Woodward, C. S., "SUNDIALS: Suite of nonlinear and differential/algebraic equation solvers," *ACM Transactions on Mathematical Software (TOMS)*, Vol. 31, No. 3, 2005, pp. 363–396. https://doi.org/10.1145/1089014.1089020.

[24] Jo, S. M., Venturi, S., Sharma, M. P., Munafò, A., and Panesi, M., "Rovibrational-Specific QCT and Master Equation Study on N2(X1g+) + O(3P) and NO(X2) + N(4S) Systems in High-Energy Collisions," *The Journal of Physical Chemistry A*, Vol. 126, No. 21, 2022, pp. 3273–3290. https://doi.org/10.1021/acs.jpca.1c10346, URL https://doi.org/10.1021/acs.jpca.1c10346, pMID: 35604650.

A. Appendix A

As reported in Sec. III.A, in the present work, the database of rates used to perform the sensitivity analysis includes only the dissociation and the exothermic ones, computed from QCT calculations. So, the recombination and the endothermic rates, *i.e.* k_i^R and $k_{ki}^{E,I}$, are computed imposing the *micro-reversibility* hypothesis (also known as *detailed balance*), by means of the equilibrium constant, K_i^{eq} and K_{ik}^{eq}, for the dissociation and for the exchange/inelastic reactions, respectively, as follows:

$$k_i^R = k_i^D \frac{1}{K_i^{eq}} = k_i^D \frac{Q_i(T) Q_{O_2}^t(T)}{\left[Q_O(T) Q_O^t(T)\right]^2}$$

$$k_{ki}^{E,I} = k_{ik}^{E,I} \frac{1}{K_{ik}^{eq}} = k_{ik}^{E,I} \frac{Q_k(T)}{Q_i(T)}$$

In this relations, Q^t represents the translational partition function, while Q_i is the internal partition function, evaluated at the translational temperature, whose expressions are:

$$Q^t(T) = \left(\frac{2\pi m K_B T}{N_A h^2}\right)^{3/2}$$

$$Q_i(T) = g_i \exp\left(-\frac{\varepsilon_i}{K_B T}\right)$$

where m represents the mass of the species, T the translational temperature, K_B the Boltzmann constant, N_A the Avogadro number and h the Planck constant.

For the time integration of the master equation, a linear implicit multi-step solver is used, as described in Sec. III.B, therefore the Jacobian needs to be provided. Being the analysis performed under the hypothesis of isochoric and isothermal 0D reactor, the analytical form of the Jacobian can be derived and it is:

$$\mathbf{J} = \begin{pmatrix} \frac{\partial F_O}{\partial Y_O} & \frac{\partial F_O}{\partial Y_j} \\ \frac{\partial F_i}{\partial Y_O} & \frac{\partial F_i}{\partial Y_j} \end{pmatrix} \qquad \text{with } i, j \in I_B \tag{30}$$

where

$$\frac{\partial F_O}{\partial Y_O} = 2 \sum_i k_i^D \left(n_i - 3\frac{n_O^2}{K_i^{eq}}\right) \qquad , \frac{\partial F_O}{\partial Y_j} = 2\frac{m_O}{m_{O_2}} \left(n_O k_j^D\right)$$

$$\frac{\partial F_i}{\partial Y_O} = -\frac{m_{O_2}}{m_O} \left(k_i^D \left[n_i - 3\frac{n_O^2}{K_i^{eq}}\right] + \sum_k k_{ik}^{E,I} \left[n_i - \frac{n_k}{K_{ik}^{eq}}\right]\right) \qquad , \frac{\partial F_i}{\partial Y_j} = -\left(n_O k_i^D \delta_{ij} + n_O \left[\sum_k \left(k_{ik}^{E,I} \delta_{ij}\right) - \frac{k_{ij}^{E,I}}{K_{ij}^{eq}}\right]\right)$$

B. Appendix B

In this part of the Appendix, the derivation of the analytical expressions for Y_{O_2} and dG/dk^D, used to verify the code in Sec. VI.A are reported.

Starting from the master Equations expression for the Macro model, here again reported:

$$\frac{dY_{O_2}}{dt} = \frac{m_{O_2}}{\rho}\left(-k^D n_O n_{O_2}\right) = -k^D n_O Y_{O_2} = f\left(Y_O, Y_{O_2}\right) \ , \tag{31}$$

$$Y_O = 1 - Y_{O_2} \qquad \text{and} \qquad n_O = \frac{\rho}{m_O} Y_O \ . \tag{32}$$

For the sake of simplicity, we define $A = \frac{\rho}{m_O} k^D$. Substituting the relations (32) into (31), the ODE becomes:

$$\frac{dY_{O_2}}{dt} = -AY_O Y_{O_2} = -A\left(1 - Y_{O_2}\right) Y_{O_2} = -A\left(Y_{O_2} - Y_{O_2}^2\right)$$

It is possible now to separate the variables and integrate them:

$$\int \frac{dY_{O_2}}{\left(1 - Y_{O_2}\right) Y_{O_2}} = \ln\left(\frac{Y_{O_2}}{1 - Y_{O_2}}\right) = -At + C_1 \implies \frac{Y_{O_2}}{1 - Y_{O_2}} = C\exp\left(-At\right) \tag{33}$$

Substituting the initial condition, $Y(t = 0) = \widetilde{Y}_{O_2}$, it is possible to compute the integration constant C, which is:

$$C = \frac{\widetilde{Y}_{O_2}}{1 - \widetilde{Y}_{O_2}} \tag{34}$$

Re-writing the expression (33), substituting the integration constant (34) and, finally, re-arranging the terms, we obtain:

$$Y_{O_2}(t) = \frac{C\exp(-At)}{1 + C\exp(-At)} = \frac{\widetilde{Y}_{O_2}\exp\left(-\frac{\rho}{m_O}k^D t\right)}{1 - \widetilde{Y}_{O_2} + \widetilde{Y}_{O_2}\exp\left(-\frac{\rho}{m_O}k^D t\right)} \tag{35}$$

Considering the objective function define by (25), we can compute the analytical sensitivity as follows:

$$\frac{dG}{dk^D} = \frac{dY_{O_2}(T_e)}{dk^D} \tag{36}$$

$$= -\frac{\rho T_e}{m_O}\frac{\widetilde{Y}_{O_2}\exp\left(-\frac{\rho}{m_O}k^D T_e\right)}{1 - \widetilde{Y}_{O_2} + \widetilde{Y}_{O_2}\exp\left(-\frac{\rho}{m_O}k^D T_e\right)} - \frac{\widetilde{Y}_{O_2}\exp\left(-\frac{\rho}{m_O}k^D T_e\right)}{\left[1 - \widetilde{Y}_{O_2} + \widetilde{Y}_{O_2}\exp\left(-\frac{\rho}{m_O}k^D T_e\right)\right]^2}$$

$$\cdot\left[-\widetilde{Y}_{O_2}\frac{\rho T_e}{m_O}\exp\left(-\frac{\rho}{m_O}k^D T_e\right)\right]$$

$$= -\frac{\rho T_e}{m_O}Y_{O_2}(T_e) + \underbrace{\frac{\widetilde{Y}_{O_2}\exp\left(-\frac{\rho}{m_O}k^D T_e\right)}{1 - \widetilde{Y}_{O_2} + \widetilde{Y}_{O_2}\exp\left(-\frac{\rho}{m_O}k^D T_e\right)}}_{Y_{O_2}(T_e)}\left[\frac{\rho T_e}{m_O}\right]\underbrace{\frac{\widetilde{Y}_{O_2}\exp\left(-\frac{\rho}{m_O}k^D T_e\right)}{1 - \widetilde{Y}_{O_2} + \widetilde{Y}_{O_2}\exp\left(-\frac{\rho}{m_O}k^D T_e\right)}}_{Y_{O_2}(T_e)}$$

$$= \frac{\rho T_e}{m_O}\left[Y_{O_2}^2(T_e) - Y_{O_2}(T_e)\right] = \frac{\rho T_e}{m_O}\left[Y_{O_2}(T_e) - 1\right]Y_{O_2}(T_e) \tag{37}$$

C. Appendix C

In this part of the Appendix, the derivation of the adjoint equations and the sensitivity expression for the different objective functions and parameters, presented in Sec. IV, are provided.
Let's first re-write the adjoint equations and the sensitivity expression from Sec. V.B:

$$\dot{\boldsymbol{\lambda}}^T \frac{\partial \mathbf{h}}{\partial \dot{\mathbf{y}}} = \boldsymbol{\lambda}^T \left(\frac{\partial \mathbf{h}}{\partial \mathbf{y}} - \frac{d}{dt} \frac{\partial \mathbf{h}}{\partial \mathbf{y}} \right) \qquad \text{Adjoint Equations}$$

$$\frac{dG}{d\mathbf{p}} (T_e) = \frac{\partial G}{\partial \mathbf{p}} + \int_0^{T_e} \boldsymbol{\lambda}^T \left(\frac{\partial \mathbf{h}}{\partial \mathbf{p}} \right) dt + \boldsymbol{\mu}^T \frac{\partial \mathbf{b}}{\partial \mathbf{p}} \qquad \text{Sensitivity}$$

where the term:

$$\mathbf{h}(\mathbf{Y}, \mathbf{Y}, \mathbf{p}, t) = \frac{d\mathbf{Y}}{dt} - \mathbf{F}(\mathbf{Y}, \mathbf{p}, t) = \mathbf{0}$$

represents the master equations in implicit form.

Moreover, the "initial" condition for the adjoint equations is to be computed, as follows:

$$\boldsymbol{\lambda}^T (t = T_e) = - \frac{\partial G}{\partial \mathbf{y}_{T_e}} \left(\frac{\partial \mathbf{h}}{\partial \dot{\mathbf{y}}} \right)^{-1}$$

A. Common terms

It is possible to notice that there are some terms, in the previous expressions, which are independent of the objective function.

In the adjoint equations, the first term, multiplying the adjoint variables vector $\boldsymbol{\lambda}^T$, is exactly the Jacobian of the system, derived in the Appendix A in the Eq. 30, with just a change of sign. In fact:

$$\frac{\partial \mathbf{h}}{\partial \mathbf{Y}} = \cancel{\frac{\partial}{\partial \mathbf{Y}} \left(\frac{d\mathbf{Y}}{dt} \right)}^{\,0} - \frac{\partial \mathbf{F}}{\partial \mathbf{Y}} = -\mathbf{J}$$

Similarly, the term $\partial \mathbf{h}/\partial \dot{\mathbf{Y}}$, present in both the adjoint equations and its initial condition, for the master equations, simplifies to:

$$\frac{\partial \mathbf{h}}{\partial \dot{\mathbf{Y}}} = \frac{\partial}{\partial \dot{\mathbf{Y}}} \left(\frac{d\mathbf{Y}}{dt} \right) - \cancel{\frac{\partial \mathbf{F}}{\partial \dot{\mathbf{Y}}}}^{\,0} = \hat{\mathbf{I}}$$

where $\hat{\mathbf{I}}$ is the identity matrix. It is straightforward to notice that the term on the right-hand side of the adjoint equations, where the time derivative of this term is present, vanishes.

In the very same fashion, the term, which multiplies the adjoint variables vector $\boldsymbol{\lambda}^T$ in the sensitivity expression, is independent of the objective function chosen. Therefore, it can be computed once for the dissociation (on the left side) and exchange/inelastic (on the right side) reaction rates:

$$\frac{\partial F_O}{\partial k_j^D} = 2 \frac{m_O}{\rho} \left(n_O n_j - \frac{n_O^3}{K_j^{eq}} \right) \qquad , \frac{\partial F_O}{\partial k_{jl}^{E,I}} = 0$$

$$\frac{\partial F_i}{\partial k_j^D} = - \frac{m_{O_2}}{\rho} \left(n_O n_i - \frac{n_O^3}{K_j^{eq}} \right) \delta_{ij} \qquad , \frac{\partial F_i}{\partial k_{jl}^{E,I}} = n_O \left[\delta_{ij} n_i - \delta_{li} n_l \right]$$

where all the indices $i, j, l \in I_{O_2}$.

Finally, since the vector of parameters $\mathbf{p}$ is not present in the initial condition of the master equations $\mathbf{b}$, then:

$$\frac{\partial \mathbf{b}}{\partial \mathbf{p}} = \hat{\mathbf{0}}$$

B. Objective function specific terms

On the other hand, the initial condition for the adjoint equations and the partial derivative of the objective function w.r.t. the parameters, present in the sensitivity expressions, need to be derived specifically for each parameter. The expression of these terms, given $G = K^D_{Glob}$, are:

$$\frac{\partial G}{\partial Y_O} = \frac{\partial}{\partial n_O}\left(\frac{\sum_i n_i k_i^D}{\sum_k n_k}\right)\frac{\partial n_O}{\partial Y_O} = 0$$

$$\frac{\partial G}{\partial Y_j} = \frac{\partial}{\partial n_j}\left(\frac{\sum_i n_i k_i^D}{\sum_k n_k}\right)\frac{\partial n_j}{\partial Y_j}$$

$$= \left[\frac{\sum_i k_i^D \delta_{ij}\left(\sum_k n_k\right) - \left(\sum_i n_i k_i^D\right)\sum_k \delta_{kj}}{\left(\sum_k n_k\right)^2}\right]\frac{\rho}{m_j}$$

$$= \left[\frac{k_j^D\left(\sum_k n_k\right) - \sum_i n_i k_i^D}{\left(\sum_k n_k\right)^2}\right]\frac{\rho}{m_j}$$

$$\frac{\partial G}{\partial k_j^D} = \frac{\partial}{\partial k_j^D}\left(\frac{\sum_i n_i k_i^D}{\sum_k n_k}\right)$$

$$= \frac{1}{\sum_k n_k}\left(\sum_i n_i \delta_{ij}\right) = \frac{n_j}{\sum_k n_k}$$

$$\frac{\partial G}{\partial k_{jl}^{E,I}} = \frac{\partial}{\partial k_{jl}^{E,I}}\left(\frac{\sum_i n_i k_i^D}{\sum_k n_k}\right) = 0$$